Real Space Imaging of Ballistic Carrier Propagation in Bi Single Crystals

J. Heil,[1] M. Primke,[1] K. U. Würz,[2] and P. Wyder[1]

[1]*Max-Planck-Institut für Festkörperforschung, Hochfeldmagnetlabor, B.P. 166, 25 Avenue des Martyrs, F-38042 Grenoble Cedex 9, France*

[2]*Physikalisches Institut der Universität, Robert-Mayer-Straße 2-4, D-65054 Frankfurt, Germany*

(Received 28 July 1994)

Carriers and phonons are excited in a small volume at the surface of a Bi single crystal by laser illumination. Their nearly ballistic propagation through the sample is studied at low temperature by real space imaging of the potential at the sample surfaces using a Cu point contact as probe electrode. A focusing of electrons due to the geometry of the Fermi surface and phonon focusing is observed. The application of a magnetic field allows the identification of the signal components. A theoretical model for the mechanism of carrier excitation and detection is proposed.

PACS numbers: 72.15.Jf, 63.20.–e, 71.25.Hc, 72.15.Eb

If pure metal crystals are cooled down to very low temperatures T, the electronic mean free path l^* can be so large that ballistic and even coherent transport through macroscopic samples with dimensions in the mm range is possible. Here, experiments in metallic single crystals [1–3] and also in semiconductor structures with two-dimensional electron systems [4] are of fundamental interest, since they probe nonclassical transport. Measurements are usually done with stationary leads to the sample and yield information about the Fermi surface (FS) and the carrier dynamics. This Letter presents a new technique for the investigation of ballistic transport of carriers and phonons in semimetals. Instead of using a fixed lead-sample geometry for the injection of nonequilibrium carriers, they are generated by the illumination of a small area on the sample surface (hot spot). They propagate through the crystal bulk and are detected by a metallic point contact (PC). Since the hot spot can be moved, this method allows real space resolved measurements of highly anisotropic transport related to the FS geometry and elastic anisotropy. Signals produced by electrons, holes, and phonons can be distinguished by their response to the application of a magnetic field B.

The direction of motion of an electron is given by its group velocity $\mathbf{v}_{gr} = \hbar^{-1}\nabla_k E(\mathbf{k})$, where $\hbar = h/(2\pi)$, h is Planck's constant, $\mathbf{k}$ is the wave vector, and $E(\mathbf{k})$ is the electron dispersion. Since the FS is a surface of constant energy (the Fermi energy E_F), $\mathbf{v}_{gr}$ is perpendicular to the FS for all FS electrons. The FS of real metals differs considerably from the free electron sphere. If directions with vanishing FS curvature exist, the electron current density exhibits singularities in these directions. This highly anisotropic transport phenomenon may be called electron focusing (EF) [5]. The surfaces of constant elastic energy in crystals are nonspherical as well, so phonon transport is anisotropic, too. This is known as phonon focusing (PF) [6,7] and has been demonstrated in numerous experiments [8]. Our technique allows the observation of EF and PF in semimetals.

The experimental setup is outlined in Fig. 1(a). A thin rectangular Bi single crystal sheet is oriented perpendicular to the z (trigonal) axis with its edges parallel to the x (binary) and y (bisectrix) axes. The samples are prepared from bulk single crystals by spark erosion and electropolishing [9]. The beam of a 15 mW Ar ion laser is chopped with a frequency between 20 and 300 Hz and coupled into an optical fiber with a core diameter of 15 μm. The fiber end is brought into a distance of several 10 μm from the sample surface. The emerging light generates a hot spot of roughly 20 μm width. About 15% of the power is coupled through the fiber. The experiments are performed in liquid ^{4}He at $1.5 \leq T \leq 4.2$ K. Cu-PC's are electrochemically etched from wires of 0.1 mm diameter. To acquire an EF pattern, a collector (C) PC is spot welded to the lower sample surface, and the fiber is scanned across

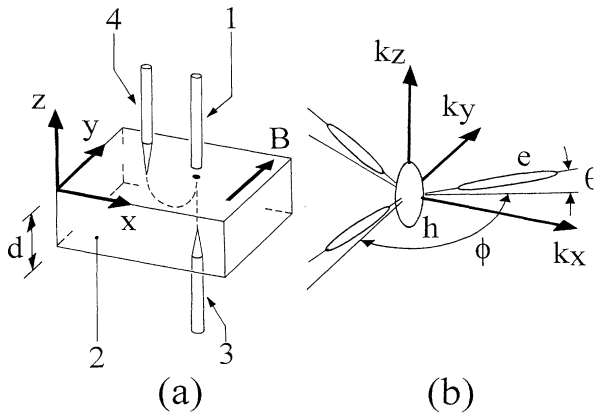

FIG. 1. (a) Experimental setup. An optical fiber (1) is used to illuminate a small area (hot spot) on the upper surface [(xy)-plane] of a Bi single crystal of thickness d (2). Cu point contacts on the lower (3) and the upper surface (4) detect the carriers excited by the laser. A magnetic field B can be applied in the (xy)-plane. (b) Fermi surface of Bi (e: electrons, h: holes, the size of the pockets is exaggerated with respect to their distance).

 0031-9007/95/74(1)/146(4)$06.00

the upper surface. The voltage V_C at C with respect to a contact on a sample edge is recorded as a function of the fiber position by lock-in detection (this is equivalent to a stationary fiber and a scanned PC).

The FS of Bi shown in Fig. 1(b) is composed of three electron ellipsoids at the L points and a hole ellipsoid at the T point of the Brillouin zone. The electron ellipsoids transform into one another by a rotation around k_z by $\phi = 120°$ [10]. Their principal half axes are $(k_{1F}, k_{2F}, k_{3F}) \approx (80, 5.3, 7) \times 10^7\ \mathrm{m}^{-1}$, the k_1 axis is inclined by $\theta \approx 6°$ against the $(k_x k_y)$ plane. The ellipsoids do not really meet the requirement of zero curvature for EF. However, they are extremely stretched along k_1 and can be approximated by cylinders, which results in EF (or at least a strong enhancement of electron flux) in the $(k_2 k_3)$ plane. $E_F \approx 23$ meV, and the effective mass for an extremal orbit around k_1 is $m^* \approx 0.01 m_e$, where m_e is the free electron mass [11].

Figure 2 displays some results for EF in Bi obtained at $T = 1.5$ K for two crystals with different thickness d. V_C is shown in grey scale as a function of the fiber position such that the electron signal appears bright. The three bright lines for $B = 0$ in Figs. 2(a) and 2(d) result from electrons of the three Fermi ellipsoids. EF occurs in planes perpendicular to k_1 due to the small FS curvature in this direction. The three EF lines do not intersect in one point because of the tilt of k_1 against the $(k_x k_y)$ plane. For $B \neq 0$ the electrons move around the FS. If the ellipsoids are approximated by cylinders with radius k_F, the corresponding real space (cyclotron) radius is $r_c = \hbar k_F / (eB \cos\alpha)$, where k_F is the Fermi wave vector, e is the electron charge, and α is the angle between B and k_1. Increasing B suppresses contributions from different ellipsoids consecutively. This is demonstrated in Fig. 2(b) for $B = 0.3$ mT along y, where only the EF line parallel to x has been suppressed. If the electron motion were purely ballistic, the center of gravity of the EF lines should be shifted for $B \neq 0$. This is not the case, so obviously some scattering exists. Even then the EF lines remain perceptible, if (intravalley) scattering within one ellipsoid dominates over (intervalley) scattering between different ones. The same applies for Fig. 2(e) for $B = 0.4$ mT along x with two suppressed EF lines. The amount of scattering suffered by the electrons cannot easily be extracted from the data in Fig. 2. However, further experiments in a different geometry described below indicate nearly ballistic transport.

In Fig. 2(c) at $B = 1.1$ mT, all EF lines are suppressed, and the dark structure, which is also visible in the other patterns, now dominates the image. It consists of an intense central spot, three straight lines spreading out radially at 120° from each other enclosed by a ringlike feature. The intensity is increased, where the lines meet the ring and at 60° from these positions. Apart from distortions caused by the nonlinearity and nonorthogonality of the cryogenic scanner mechanics, the

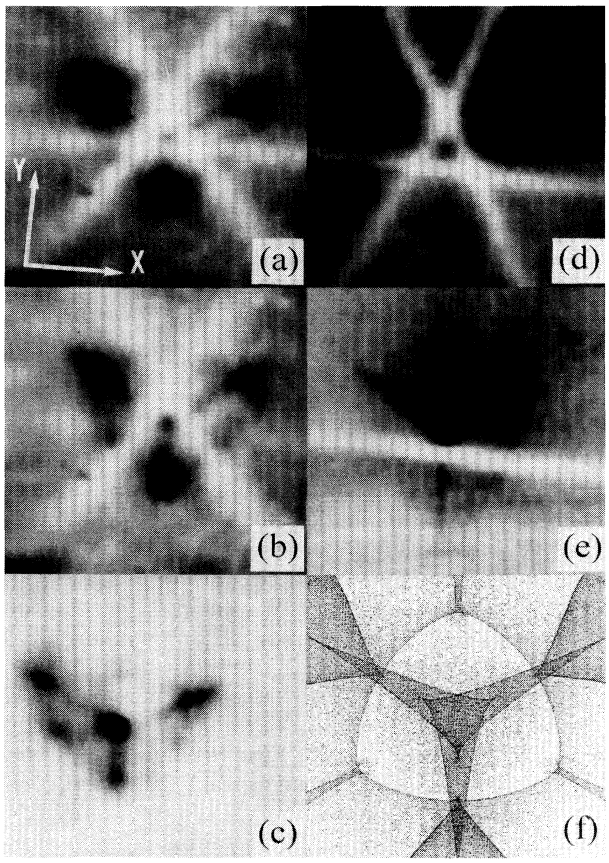

FIG. 2. Electron focusing (EF). V_C is shown in grey scale as a function of the fiber position (50 × 50 raw data) for a crystal with $d \approx 0.2$ mm in (a), (b), and (c) and $d \approx 0.5$ mm in (d) and (e). (a) The image frame is $\approx (0.5\ \mathrm{mm})^2$, the bright lines correspond to electron signals, $40 \leq V_C \leq 160$ nV, $T = 1.5$ K, and $B = 0$. (b) Like (a) but $B = 0.3$ mT, $B \parallel y$. (c) Like (a) but $B = 1.1$ mT, $B \parallel y$; a tilt produced by stray fields has been removed. (d) $d \approx 0.5$ mm, the image size is $\approx (1\ \mathrm{mm})^2$, $6 \leq V_C \leq 20$ nV. (e) Like (d) but $B = 0.4$ mT, $B \parallel x$. (f) Calculated phonon focusing (PF) pattern for ST phonons, the image frame is $(2d)^2$ corresponding to that of (d) and (e). Dark areas represent regions with high phonon intensity.

structure exhibits threefold symmetry. Figure 2(f) shows a theoretical PF image for slow transverse (ST) phonons obtained by a Monte Carlo calculation performed with the elastic constants of Bi [12]. It was done using a random choice of 10^6 k vector directions and the calculation of the corresponding group velocities [13]. The general features of the dark structures in Figs. 2(a)–2(e) correspond quite well to the part of Fig. 2(f) within the ring, apparently being related to the focusing of ST phonons.

The PC is phonon-sensitive for several reasons. Phonons heat up the surface, presumably produce a thermal gradient in the PC, and drag carriers from the hot spot toward and through the PC (phonon drag). These effects

generate a (thermoelectric) voltage at the Bi/Cu-PC [14,15]. Further experiments to identify the responsible mechanisms are required. It is not clear why no signals are detected outside the ring feature. Ballistic ST phonons in Bi have been reported along k_z at $T \approx 1.4$ K, changing into second sound for $T \rightarrow 4.2$ K [16].

Figure 3 presents data recorded with C placed on the upper surface near the hot spot. A field $B = 0.5$ mT is applied along y. All electron trajectories are bent back to the upper surface. This image represents a spatially resolved version of transverse electron focusing (TEF) [2,3]. We will refer to this technique using the term light induced TEF (LITEF). In TEF electrons are injected into a crystal through an emitter (E) PC at $x = 0$ with an excess energy up to eV_E, where V_E is the voltage at E. Their trajectories accumulate in caustics, giving rise to a peak in the voltage pattern at the surface at $x = 2r_c$, which can be detected with C positioned at $x = L$ while sweeping B (in Bi $r_c \approx 5 \times 10^{-8} B^{-1}$ mT, L is the distance between E and C). Electrons are reflected at surfaces, so they give rise to a series of peaks. Since TEF is well understood, it may help to explain our EF results.

Figure 4 compares $V_C(B)$ recorded employing TEF [Fig. 4(a)], LITEF [Figs. 4(c) and 4(d)], and the corresponding theoretical curves [Figs. 4(b) and 4(e)]. Both methods yield series of focusing peaks for $B > 0$. However, there are two major differences.

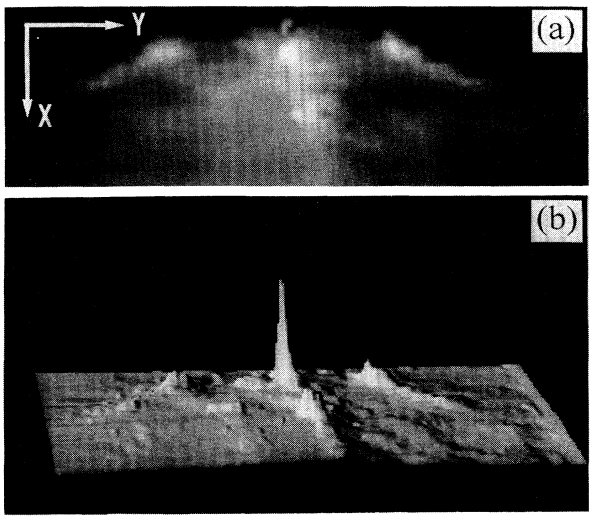

FIG. 3. Light induced transverse electron focusing (LITEF), C is positioned on the upper sample surface at the common point of intersection of the three bright electron traces, $d = 2$ mm, $B = 0.5$ mT, $B \parallel y$. (a) V_C in grey scale representation as a function of the fiber position. A tilt produced by stray fields has been removed. $\triangle y = 1.5$ mm, $\triangle x = 0.5$ mm, $0 \leq V_C \leq 100$ nV, and $T = 1.5$ K. (b) The same data given in a perspective representation.

First, the sign of the signal for $B \leq 0$, which is generated by holes, is opposite for the two techniques. In TEF they are injected in antiphase to electrons. The lock-in detection then yields signals of equal sign for both. In LITEF electrons and holes are excited simultaneously during the half period of the excitation cycle, in which the chopper is open. Here, electrons and holes give rise to signals of opposite polarity.

Second, the peak shape is different for both methods. For isotropic injection, $T = 0$, $l^* \rightarrow \infty$, infinitesimal size of E and C, $V_E \rightarrow 0$ and cylindrical FS, the theoretical TEF line shape is $V_C(k_F) \sim x/(2r_c)^2\{1 - [x/(2r_c)]^2\}^{-1/2}$ [2,3]. Here, only electrons from an infinitesimal k layer around k_F contribute. A typical TEF line rises smoothly with increasing B up to the so-called focusing field B_f, above which it drops abruptly [$2r_c(B_f) = L$]. A LITEF line starts with a negative slope, shows a minimum, then a large maximum at $B \approx B_f$, followed by a slow decay.

For simplicity we assume that the only effect of laser illumination is that of heating the hot spot up to T_h, leaving the rest of the sample cold at T_c. At finite $T_{h,c}$ and V_E, the electron system is described by the Fermi distribution function $f_{\pm,h,c} = f(E \pm eV_E/2, T_{h,c})$. For $E(k) \sim k^2$, $f_{\pm,h,c}$ can be expressed in terms of k. Since $r_c = r_c(k)$, every k layer produces its proper $V_C(k)$. The total V_C follows by summing over all

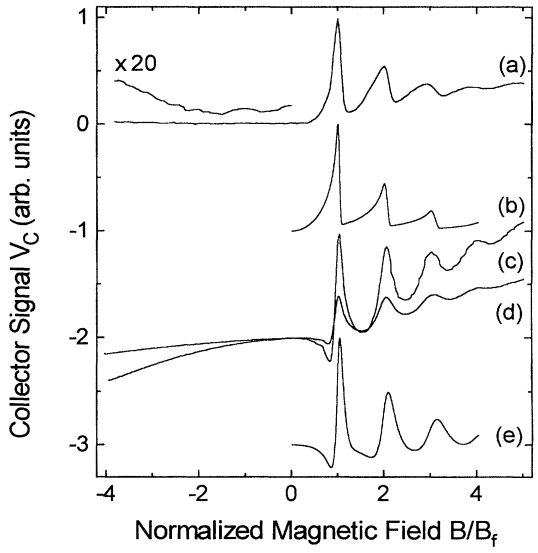

FIG. 4. TEF and LITEF signals for C positioned at $x = L = 0.2$ mm as a function of the magnetic field B normalized to the focusing field B_f. (a) TEF data for $V_E = 2$ mV, the signal level is $V_C \leq 100$ nV. (b) Theoretical TEF characteristic for $T = 1.5$ K, $V_E = 2$ mV, $l^* \rightarrow \infty$, $q = 0.4$, extension of E, $C \rightarrow 0$. (c), (d) LITEF data for $T = 1.5$ K and $T = 4.2$ K. The signal level is $V_C \leq 100$ nV. (e) Theoretical LITEF characteristic for $T_h = 30$ K, $T_c = 1.5$ K, $l^* \rightarrow \infty$, $q = 0.5$, extension of hot spot: 20 μm, extension of $C \rightarrow 0$. The curves are separated by individual offsets.

layers: $V_C \sim \int_0^\infty [f_{+,h} - f_{-,c}] V_C(k) k^2 \, dk$, band structure effects are neglected, $V_C = V_C(x, B, V_E, T_{h,c})$. One k enters the integrand because the current carried by each state is proportional to its k (two-dimensional), k space integration yields another k.

A TEF characteristic is calculated with $V_E \neq 0$ and $T_h = T_c$; the result is shown in Fig. 4(b). V_C is summed up for multiple reflections at the surface assuming $l^* \to \infty$. The probability for specular reflection is set to $q = 0.4$. Apart from the background (given by diffusely reflected electrons, which are dropped for simplicity), the general features agree well with the experimental result. A LITEF characteristic follows with $V_E = 0$ and $T_h > T_c$. Again, the result displayed in Fig. 4(e) is in qualitative agreement with the experiment. Here, $q = 0.5$. The hot spot is modeled by a Gaussian of 20 μm width. The parameters should not be taken very seriously because of the crude model. The negative onset of the line is of particular interest. Here no holes, but electrons are focused to C. They are excited thermally from $E < E_F$ to $E > E_F$. Consequently they are missing at $B < B_f$ and appear at $B > B_f$. The signal at $B < 0$ is not described by our model. The hole mean free path is much shorter than that of electrons [17]. Therefore the holes do not yield a peak series, but a somewhat averaged signal.

The model is certainly oversimplified, but apparently the assumption of ballistic transport of thermally excited carriers corresponds well to the experimental situation [at least $l^* \approx L (\approx d)$ applies]. The signal increases with the range Δk over which the FS is smeared out thermally. For a parabolic band $\Delta k \sim T_h / \sqrt{E_F}$, this favors semimetals with small E_F for this kind of experiment. In the context of thermoelectricity, the data presented here can be seen as ballistic counterparts of the Seebeck, Thomson ($B = 0$, EF) and the Nernst-Ettinghausen ($B \neq 0$, LITEF) effects and their composition from carrier and phonon drag contributions [14,15].

In conclusion, we have presented a new technique to study the (nearly) ballistic propagation of thermally excited carriers through semimetal crystals. The potential pattern on the sample surfaces generated by the ballistic carriers is studied in real space. EF due to the FS geometry of Bi is observed. The influence of T and B on the patterns is studied. A ballistic phonon pattern is observed. A theoretical model for the mechanism of the signal generation is presented. This new technique yields complementary information to existing methods for FS investigation [18,19], namely, directions of vanishing FS curvature. The carriers show a thermal spectrum, so information about $E(\mathbf{k})$ seems accessible. The technique allows the observation of carriers (and phonons) at specific $\mathbf{k}$, so E- and $\mathbf{k}$-resolved studies of the interaction of carriers with external fields and excitations (like ultrasound, carriers, and phonons from a second hot spot or PC) seem possible. The mean free path of carriers and their interaction with surfaces and interfaces can be investigated directly. Similar experiments with carriers in semiconductors and quasiparticles in superconductors seem feasible.

We wish to thank E. Schönherr, H. Wendel, and H. Bender from M. P. I.-Stuttgart for supplying the Bi-crystals, R. Hock for the recipe for Bi-electropolishing, R. Cinti for supplying equipment, and J. Wesner, W. Grill, and A. G. Every for helpful discussions.

[1] Yu. V. Sharvin and L. M. Fisher, Zh. Eksp. Teor. Fiz. Pis'ma Red. **1**, 54 (1965) [JETP Lett. **1**, 152 (1965)].
[2] V. S. Tsoi, Zh. Eksp. Teor. Fiz. Pis'ma Red. **19**, 114 (1974) [JETP Lett. **19**, 70 (1974)].
[3] V. S. Tsoi, J. Bass, and P. Wyder, Adv. Phys. **41**, 365 (1992).
[4] C. W. J. Beenakker and H. van Houten, Solid State Phys. **44**, 1 (1991).
[5] A. M. Kosevich, Sov. J. Low Temp. Phys. **11**, 611 (1985).
[6] F. Rösch and O. Weiss, Z. Phys. B **25**, 101 (1976).
[7] A. G. Every, Phys. Rev. B **34**, 2852 (1986).
[8] R. L. Weaver, M. R. Hauser, and J. P. Wolfe, Z. Phys. B **90**, 27 (1993).
[9] Electrolyte: saturated aqueous KI-solution +2% vol HCl, cathode: C, $V_{DC} = 7$ V.
[10] E. Fawcett, R. Griessen, W. Joss, and W. Kress, in *Metals: Phonon States and Electron States and Fermi Surfaces,* edited by K. H. Hellwege and J. L. Olsen, Landolt-Börnstein, New Series, Group 3, Vol. 13, Pt. b (Springer-Verlag, Berlin, 1983); A. P. Cracknell, in *Electron States and Fermi Surfaces of Elements,* edited by K. H. Hellwege and J. L. Olsen, Landolt-Börnstein, New Series, Group 3, Vol. 13, Pt. c (Springer-Verlag, Berlin, 1984).
[11] V. S. Edelman, Adv. Phys. **25**, 555 (1976).
[12] V. A. Šutilov, *Physik des Ultraschalls* (Akademie-Verlag, Berlin, 1984).
[13] G. A. Northrop, Comput. Phys. Commun. **28**, 103 (1982).
[14] D. K. C. MacDonald, *Thermoelectricity* (Wiley, New York, 1962).
[15] R. D. Barnard, *Thermoelectricity in Metals and Alloys* (Taylor & Francis, London, 1972).
[16] V. Narayanamurti and R. C. Dynes, Phys. Rev. Lett. **28**, 1461 (1972).
[17] I. F. Sveklo and V. S. Tsoi, Zh. Eksp. Teor. Fiz. **103**, 1705 (1993) [Sov. Phys. JETP **76**, 839 (1993)].
[18] D. Shoenberg, *Magnetic Oscillations in Metals* (Cambridge Univ. Press, Cambridge, 1984).
[19] A. P. Cracknell and K. C. Wong, *The Fermi-Surface* (Clarendon Press, Oxford, 1973).

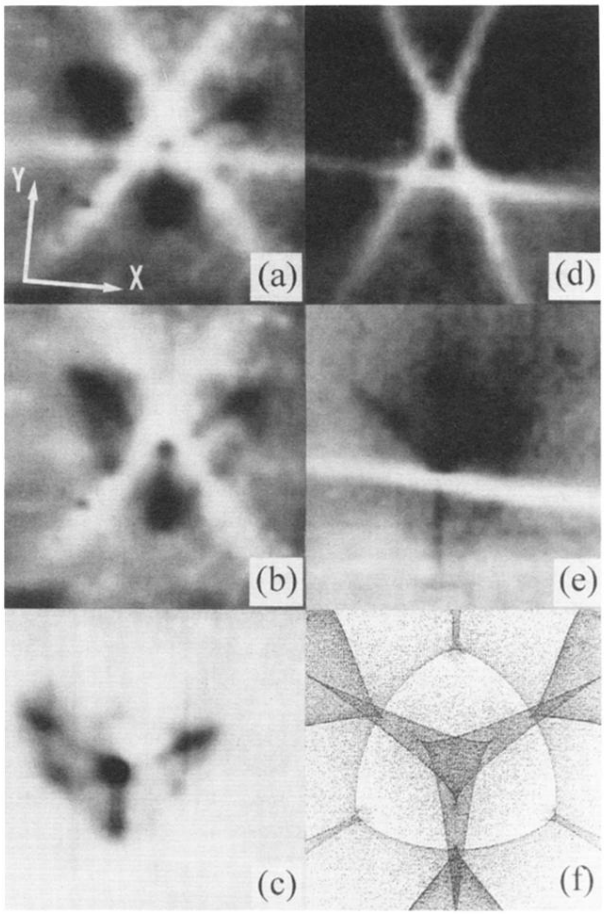

FIG. 2. Electron focusing (EF). V_C is shown in grey scale as a function of the fiber position (50×50 raw data) for a crystal with $d \approx 0.2$ mm in (a), (b), and (c) and $d \approx 0.5$ mm in (d) and (e). (a) The image frame is $\approx (0.5\ \text{mm})^2$, the bright lines correspond to electron signals, $40 \leq V_C \leq 160$ nV, $T = 1.5$ K, and $B = 0$. (b) Like (a) but $B = 0.3$ mT, $B \parallel y$. (c) Like (a) but $B = 1.1$ mT, $B \parallel y$; a tilt produced by stray fields has been removed. (d) $d \approx 0.5$ mm, the image size is $\approx (1\ \text{mm})^2$, $6 \leq V_C \leq 20$ nV. (e) Like (d) but $B = 0.4$ mT, $B \parallel x$. (f) Calculated phonon focusing (PF) pattern for ST phonons, the image frame is $(2d)^2$ corresponding to that of (d) and (e). Dark areas represent regions with high phonon intensity.

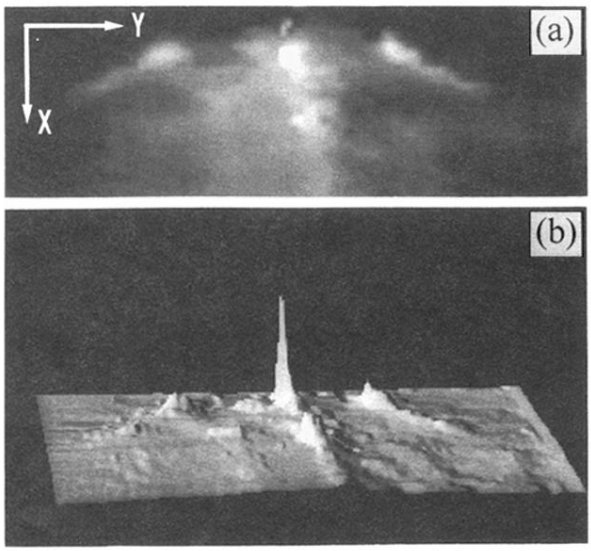

FIG. 3. Light induced transverse electron focusing (LITEF), C is positioned on the upper sample surface at the common point of intersection of the three bright electron traces, $d = 2$ mm, $B = 0.5$ mT, $B \parallel y$. (a) V_C in grey scale representation as a function of the fiber position. A tilt produced by stray fields has been removed. $\triangle y = 1.5$ mm, $\triangle x = 0.5$ mm, $0 \leq V_C \leq 100$ nV, and $T = 1.5$ K. (b) The same data given in a perspective representation.